Tunable Asymmetric Magnetoresistance in Fe₃GeTe₂/Graphite/Fe₃GeTe₂ Lateral Spin Valve

Supporting Information

Xiangyu Zeng,[a,b,‡] Ge Ye,[c,‡] Fazhi Yang,[d] Qikai Ye,[e] Liang Zhang,[f] Boyang Ma,[e] Yulu Liu,[e] Mengwei Xie,[c] Yan Liu,[a,b]* Xiaozhi Wang,[e]* Yue Hao,[a,b] and Genquan Han,[a,b]

[a]Hangzhou Institute of Technology, Xidian University, Hangzhou, 311200, China

[b]State Key Discipline Laboratory of Wide Band Gap Semiconductor Technology, School of Microelectronics, Xidian University, Xi'an 710071, China.

[c]Center for correlated matter and Department of Physics, Zhejiang University, Hangzhou, 310027, China

[d]Beijing National Laboratory for Condensed Matter Physics and Institute of Physics, Chinese Academy of Sciences, Beijing 100190, China

[e]College of Information Science and Electronic Engineering, Zhejiang University, Hangzhou, 310027, China

[f]Research Center for Humanoid Sensing and Perception, Zhejiang Lab, Hangzhou, 311100, China

*Corresponding Authors

XiaoZhi Wang - College of Information Science and Electronic Engineering, Zhejiang University, Hangzhou, 310027, China. Email: xw224@zju.edu.cn

Yan Liu - Hangzhou Institute of Technology, Xidian University, Hangzhou 311200, China. Email: xdliuyan@xidian.edu.cn

Section S1. The thicknesses of different layers

The thicknesses of Graphite, FGT 1, and FGT 2 are measured as 9.7, 42, and 22.5 nm, respectively, as depicted in **Figure S1a**, Figure **S1b**, and Figure **S1c**.
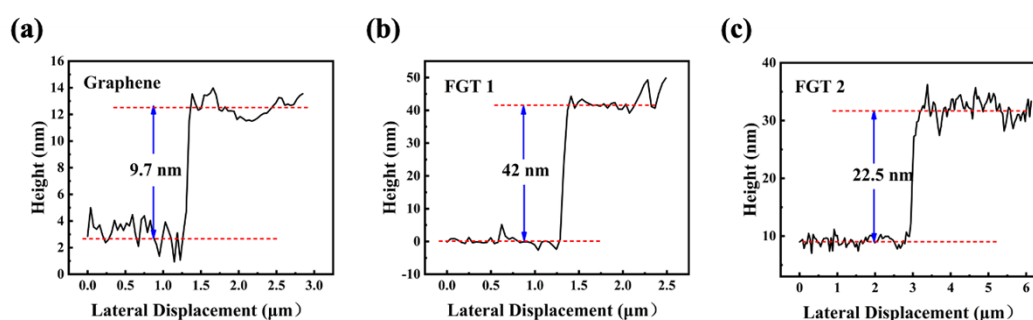
Figure S1. The thicknesses of different layers.

Section S2. The transport behaviors of the device

The device resistance increases with the drop of temperature from 300 to 2 K as exhibited in **Figure S2a**. This behavior is different from that of the intrinsic FGT[1] which was characterized in our previous work showing a resistance decrease but much similar to the graphite[2]. Thus, the graphite layer is determined to dominate the junction's resistance behavior.

Figure S2b shows the raw data of the spin valve's transport properties that are measured at different temperatures. The rapidly increasing magnetoresistance baselines strongly obstruct the analysis of the temperature dependence of the resistance platform height, thus, they are subtracted and replotted in **Figure 1b**.
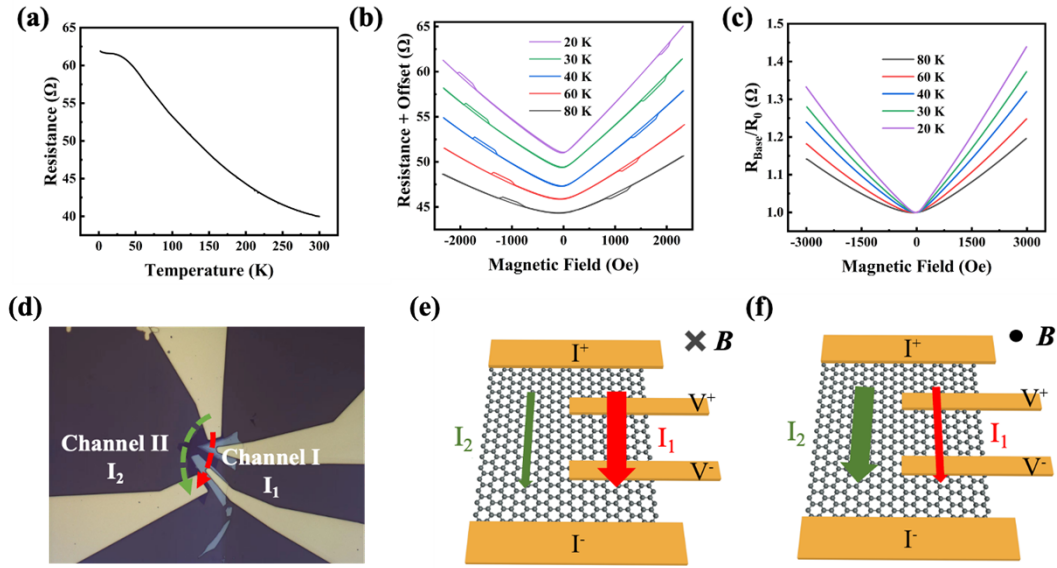
Figure S2. The transport behaviors of the device. (a) The junction resistance changes with the drop of temperature from 300 to 2 K; (b) The transport properties measured at different temperatures; (c) The baselines of the magnetoresistance measured at different temperatures; (d) Two current channels in the as-fabricated device; the schematic diagrams of the current distribution when a positive or a negative magnetic field is applied are illustrated in (e) and (f), respectively.

The baselines of the transport curves measured at different temperatures are displayed in **Figure S2c** with a positive magnetoresistance behavior. As reported in our previous research, 2D FGT flakes of different thicknesses present linear negative magnetoresistance, however, graphite shows a positive magnetoresistance at low temperature[2]. Thus, the graphite layer mainly dominates the junction resistance, fitting well with the analysis of the device resistance cooling curve.

The obtained magnetoresistance curves are asymmetry to the zero magnetic fields. For instance, at 30 K, the resistance measured at 3000 Oe is 59.66 Ω, 4.16 Ω higher

than that measured at -3000 Oe. This resistance asymmetry is similar to the phenomenon reported in the van der Pauw geometry[2], which is attributed to the asymmetry of two different current channels. In detail, since the two FGT layers of the as-fabricated device do not traverse the graphite layer, the current channel can be divided into two parallel parts, as shown in **Figure S2d.** The current flow under the FGT ferromagnetic electrode is defined as I_1 and the corresponding current channel is named Channel I (marked by the red dash line in **Figure S2d**). The rest of the current and corresponding current channel is defined as I_2 and Channel II (marked by the green dash line in **Figure S2d**), respectively. Obviously, only the voltage drops (V) in Channel I can be measured, however, the device resistance is calculated using the total applied current as follows: $V/(I_1+I_2)$; When a positive magnetic field is applied, as shown in **Figure S2e**, the Lorentz force moves most of the carriers to Channel I increasing I_1 to larger than I_2, correspondingly, the measured V is higher. Conversely, I_2 becomes higher than I_1 as a negative magnetic field is applied (**Figure S2f**) and a lower V is obtained. Thus, since the total applied current maintain unchanged, the calculated resistance with a positive field is higher than that with a negative field.

Section S3. The four-prob resistance measurement

In the four-prob method, there are two current loops during the device resistance measurement, as shown in **Figure S3**. Since the resistance of the voltmeter (R_V) is extremely high, the current passing the heterojunction (I_h) can be approximated as the current flowing through the ammeter, and the accurate resistance of the heterojunction (R_h) can be obtained. However, if the wire resistance (R_w) and the contact resistance

(R_c) in the voltmeter loop are comparable to R_h, the measured voltage by the voltmeter will be significantly affected by the change of R_c. In this work, the R_h and R_c+R_w of the two-layer device are both tens of Ohms, thus, the variation of R_c+R_w with the magnetic field change can be observed.
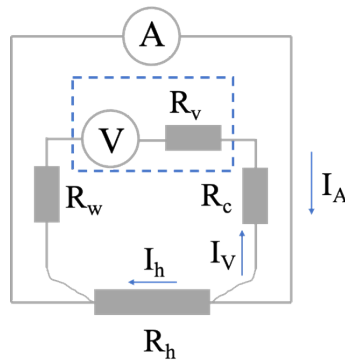
Section S3. The schematic diagram of the four-prob method for the device resistance measurement.

Section S4. The working principle of the two-layer device

The magnetoresistance behavior of the device measured at 80 K is similar to that at 40 K, as displayed in **Figure S4a**. The device shows a "High to low" and "Low to High" resistance switch in the negative and positive sweep, respectively, when the FGT layer faces upward.
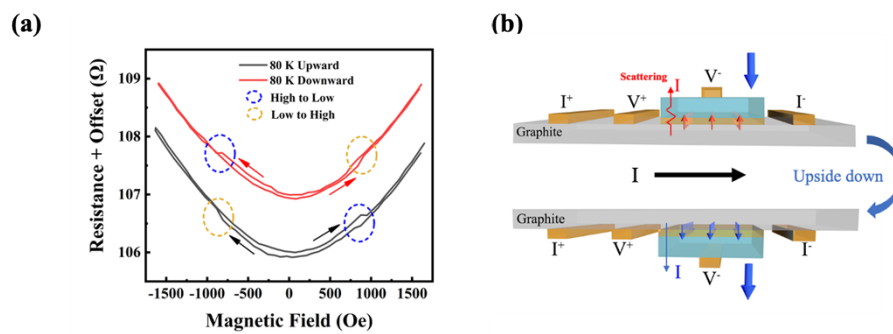
Figure S4. The working principle of the two-layer device. (a) The schematic diagram

of the working principle of the two-layer device; (b) The magnetoresistance measured with different device surface orientations at 80 K.

Figure S4b presents the working mechanism of the device with the FGT magnetized downward. A positive magnetic field is applied initially to ensure the FGT is magnetized upward as illustrated in the main text. With the magnetic field increasing negatively to higher than the FGT layer's coercive field, the magnetization direction of the FGT layer switches downward which is opposite to the interface (spin up), as shown in the upper part of **Figure S4b**. Thus, electrons will suffer a strong spin-dependent scattering between the interface and the FGT layer, leading to the two-layer device exhibiting a higher resistance state. After the device is turned upside down, both the FGT layer and the interface is spin-down, therefore, electrons can pass through freely and the device stays in the low resistance state, as depicted in the lower part of **Figure S4b**.

Section S5. The transport properties of the spin valve.

Since the current is applied from the right to the left, the spin momentums of the two interfaces maintain facing downward. When FGT 1 and FGT 2 are both magnetized upward, as presented in **Figure S5a**, V_{spin} generates in both two interfaces and the measured voltage can be expressed as $V=\varphi_2 - \varphi_4 = (\varphi_1 - V_{spin}) - (\varphi_3 - V_{spin}) = \varphi_1 - \varphi_3 = -\Delta V$. Similarly, while FGT 1 and FGT 2 are magnetized downward (**Figure S5b**), electrons can pass through the interfaces to FGT 1 or FGT 2 freely, and $V = \varphi_2 - \varphi_4 = \varphi_1 - \varphi_3 = -\Delta V$.
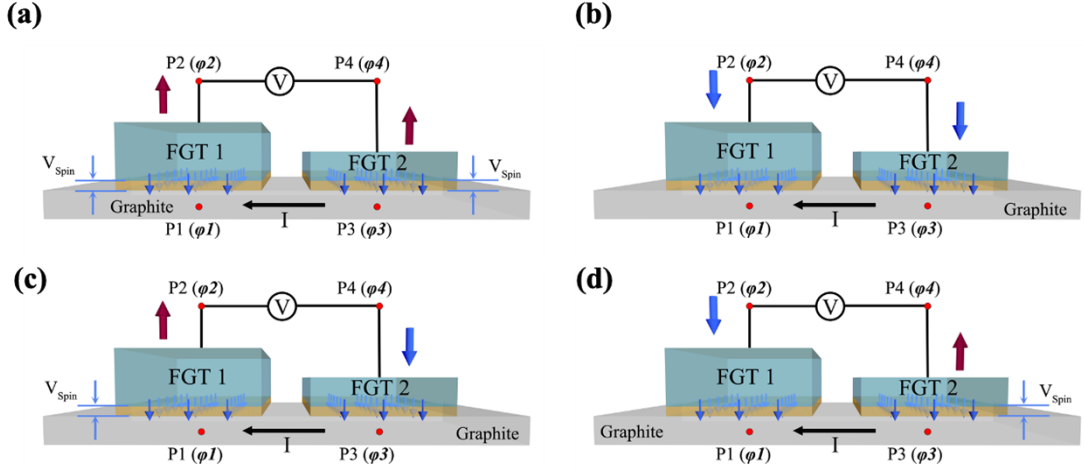
Section S5. The schematic diagram of the working mechanism with the current flowing from the right to the left. The working mechanisms of the spin valve with two FGT layers magnetized parallel are shown in (a) and (b), and those for antiparallel configurations are shown in (c) and (d).

When FGT 1 and FGT 2 are magnetized upward and downward (**Figure S5c**), respectively, V_{spin} only appears in Interface I, and $V = \varphi_2 - \varphi_4 = (\varphi_1 - V_{spin}) - \varphi_3 = -\Delta V - V_{spin} = -(\Delta V + V_{spin})$. Conversely, when FGT 1 and FGT 2 are magnetized downward and upward, respectively (**Figure S5d**), V_{spin} only generates in Interface I, thus, V can be expressed as $V = \varphi_2 - \varphi_4 = \varphi_1 - (\varphi_3 - V_{spin}) = -\Delta V + V_{spin} = -(\Delta V - V_{spin})$.

For the applied current is negative (–I) in this circumstance, the resistance calculated with two FGT layers in P configurations can be written as $(-\Delta V)/(-I) = \Delta V/I$. In addition, the resistances presented in **Figure S5c** and **Figure S5d** are $-(\Delta V + V_{spin})/(-I) = (\Delta V + V_{spin})/I$, and $-(\Delta V - V_{spin})/(-I) = (\Delta V - V_{spin})/I$, respectively. These calculated resistances with different FGT magnetized configurations are all the same as

those measured with the opposite current direction, consequently, the device magnetoresistance behavior maintains unchanged.

Section S6. The transport behavior of the oxide spin valve

The raw data of the oxidized device's transport properties are displayed in **Figure S6a**. The resistance platform width decreases firstly with the temperature drop from 80 K to 20 K, and then begins to increase ever after, as displayed in **Figure S6b**. The current dependence of the device magnetoresistance behavior is measured with the applied current increase from 0.01 μA to 20 μA, as summarized in **Figure S6c**. The device maintains a similar property under different applied currents, however, the signal-to-noise ratio becomes larger with the current increase.
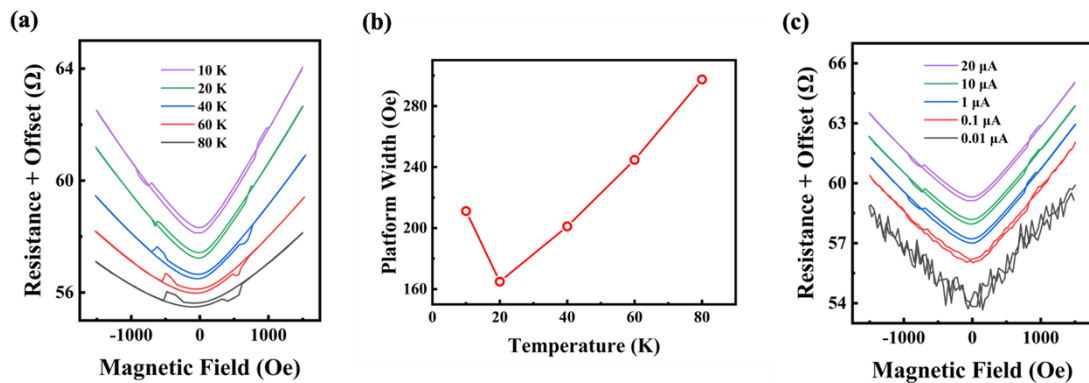
Section S6. The transport behavior of the oxide spin valve. (a) The temperature dependence of the oxidized device's transport properties; (b) The platform width's change with the temperature; (c) The current dependence of the spin valve.

Section S7. The four resistance states in the transport property of the oxidized device.

As illustrated in **Figure S7**, the spin potential drops in FGT1/graphite and FGT2/graphite interfaces are termed V_{spin1} and V_{spin2}, respectively. The measured

voltages with FGT 1 and FGT 2 in the magnetization configuration of up-up (**Figure 3a**), down-down (**Figure 3b**), up-down (**Figure 3c**), and down-up (**Figure 3d**) can be written as ΔV, $\Delta V - V_{spin1} + V_{spin2}$, $\Delta V + V_{spin2}$, and $\Delta V - V_{spin1}$, respectively. For the device measured before the oxidation process, V_{spin1} is almost equal to V_{spin2}, and $\Delta V - V_{spin1} + V_{spin2} = \Delta V$. The device exhibits three resistance states.

After the oxidation processes, the coupling between antiferromagnetic and ferromagnetic may affect the spin-orbital coupling in the FGT layer, and finally modulate the spin-momentum locking effect. Since the FGT 1 and FGT 2 have different thickness ratios between the FGT and the O-FGT layer after the oxidation process, the influence on the spin-momentum locking effect is different, consequently, the value of V_{spin1} is different from V_{spin2} and the device displays four resistance states.
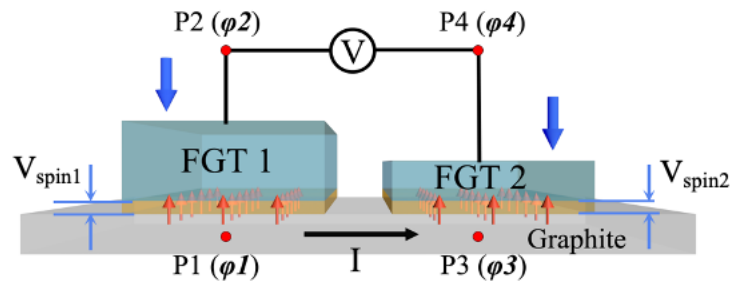
Figure S7. The working principle of the spin valve device with both FGT 1 and FGT 2 magnetized downward.

REFERENCES

1. X. Zeng, G. Ye, S. Huang, L. Zhang, H. Xu, Y. Liu, H. Kuang, B. Ma, J. Luo, X. Lu and X. Wang, *J Phys Condens Matter*, 2022, **34**.

2. J. Lu, H. Zhang, W. Shi, Z. Wang, Y. Zheng, T. Zhang, N. Wang, Z. Tang and P.

Sheng, *Nano Lett*, 2011, **11**, 2973-2977.